

# Magnetic order of Cr thin films in Nb/Cr/Fe-nanoisland hybrid: A comparative study between magnetic and superconducting properties

E. Navarro,<sup>1,a)</sup> M. Vélez,<sup>2</sup> Y. Huttel,<sup>3</sup> A. Pérez Junquera,<sup>2</sup> J. I. Martín,<sup>2</sup> O. F. de Lima,<sup>1,b)</sup> A. Cebollada,<sup>4</sup> J. M. Alameda,<sup>2</sup> and J. L. Vicent<sup>1</sup>

<sup>1</sup>*Departamento de Física de los Materiales, Facultad Ciencias Físicas, Universidad Complutense de Madrid, 28040 Madrid, Spain*

<sup>2</sup>*Departamento de Física, Facultad de Ciencias, Universidad de Oviedo–CINN, 33007 Oviedo, Spain*

<sup>3</sup>*Instituto de Ciencia de Materiales de Madrid (ICMM), CSIC, 28049 Cantoblanco, Madrid, Spain*

<sup>4</sup>*Instituto de Microelectrónica de Madrid (IMM), CNM, CSIC, 28760 Tres Cantos, Madrid, Spain*

(Received 9 October 2008; accepted 18 December 2008; published online 10 February 2009)

Shifted hysteresis loops characteristic of the exchange bias effect between a ferromagnet and an antiferromagnet are demonstrated in structures formed by a 2.5 nm Cr layer deposited on top of an array of Fe nanoislands (Cr/Fe-nanoislands). This effect evidences the persistence of antiferromagnetic (AF) order for Cr layers much thinner than the thickness reported in the literature. The field shift measured is found to increase for the smallest island sizes, which can be related with the enhancement of the Fe-nanoisland surface to volume ratio. The comparative study between superconducting proximity effects in Nb/Cr/Fe-nanoislands and Nb/normal metal/Fe-nanoisland hybrids (where the normal metals used are Al and Pt) confirms the presence of AF order in the 2.5 nm Cr spacer layer. A much shorter penetration depth of the Cooper pairs into the AF Cr layers than in the normal metal Pt and Al spacer layers is deduced. © 2009 American Institute of Physics. [DOI: 10.1063/1.3075740]

## I. INTRODUCTION

Thin film magnetism has long been a subject of interest and intense research activity since the magnetic properties of thin films present important differences from the properties of the bulk material. Many interesting physical phenomena have been described in magnetic multilayers such as the oscillating exchange coupling of ferromagnetic films across nonferromagnetic spacer layers. The Fe/Cr system has deserved particular attention since the discoveries of antiferromagnetic (AF) coupling between Fe films separated by a thin Cr layer and of giant magnetoresistance in Fe/Cr multilayers.<sup>1</sup> Previously, the focus of interest was mainly the magnetic properties of the Fe layers but, more recently, interest has shifted toward the study of antiferromagnetism of the Cr spacer layer.<sup>2–4</sup>

Bulk Cr is an itinerant antiferromagnet<sup>5</sup> displaying an incommensurate spin density wave below the Néel temperature ( $T_N=311$  K), but the magnetic properties of Cr thin films are turned aside remarkably from the Cr bulk case. A loss of the magnetic properties of the Cr thin films when the thickness decreases below 4 nm has been reported by some authors,<sup>6</sup> while others<sup>7</sup> maintain that the incommensurate spin density wave of the bulk phase becomes commensurate for thickness below 4–5 nm. Actually it is clear that in thin films, the magnetic state of Cr is strongly affected by electronic and magnetic boundary conditions.<sup>8</sup> For example, the magnetic properties of Cr thin films depend on how they are integrated in structures such as bilayers, trilayers, or multilayers and on the structural lattice mismatch,<sup>9</sup> the disorder,

the roughness or the steps in the interface,<sup>10</sup> the crystalline direction,<sup>11</sup> and the interdiffusion.<sup>2,12</sup> Also the formation of disordered alloys<sup>13</sup> in the interface can generate frustrations which can substantially suppress the magnetic moment of some Cr atoms.

In the present paper we have focused on the effect of disorder and roughness on the magnetic properties and on the exchange bias effect in Cr/Fe bilayers where the ferromagnetic film is replaced by a layer consisting of an assembly of Fe nanoislands. In previous works we demonstrated the conformal nature of Pt and Al overlayers deposited onto Fe nanoislands<sup>14</sup> and the formation of alloys at the interfaces between these overlayers and the Fe-nanoisland surfaces.<sup>15</sup> Alloying processes in these systems with reduced dimensions are likely to be mandatory for their magnetic properties. The same conformal character of Cr layer grown onto Fe-nanoisland surface is observed which provides a highly distorted Cr–Fe interface. In this work we show how this complex Cr/Fe-nanoisland geometry is responsible for both the AF order and the exchange bias effect observed for Cr layer thickness much lower than the critical thickness reported in the literature.

In addition in the present paper we approach the problem of the magnetic property determination of Cr thin films from a different point of view. We have deposited a superconducting Nb layer onto the Cr/Fe-nanoisland bilayer in order to analyze the superconducting proximity effect in Nb/Cr/Fe-nanoisland hybrids. Recently, proximity effects between superconductors and magnetic materials have been the focus of the attention of a lot of researchers since they involve the interplay and competition between two long range order effects: magnetism and superconductivity.<sup>16</sup> Many experimental studies in different combinations of ferromagnetic/

<sup>a)</sup>Electronic mail: enavarro@fis.ucm.es.

<sup>b)</sup>On leave from Inst. Fis. Gleb Wataghin, Univ. Estadual de Campinas, BR-13083 Campinas, SP, Brazil.

TABLE I. Morphological characteristics of the fabricated Fe island/spacer/Nb film structures indicating nominal layer thicknesses and materials, average island size, and height obtained from AFM characterization, and  $S_{\text{isl}}/S_{\text{subs}}$  and  $S_{\text{isl}}/V_{\text{isl}}$  ratios estimated with a cylindrical island model.

Nb thickness (nm)	Spacer layer	Nominal Fe thickness (nm)	Island diameter (nm)	Island height (nm)	$S_{\text{isl}}/S_{\text{subs}}$	$S_{\text{isl}}/V_{\text{isl}}$ ( $\text{nm}^{-1}$ )
25	2.5 nm Al	0.8	12.4	2.2	1.71	0.77
25	2.5 nm Pt	0.8	12.5	2.3	1.74	0.75
25	2.5 nm Cr	0.8	12.4	2.3	1.74	0.75
25	2.5 nm Al	2.4	30	7.1	1.95	0.27
25	2.5 nm Pt	2.4	30	7.1	1.95	0.27
25	2.5 nm Cr	2.4	30	7.0	1.93	0.28
25	2.5 nm Cr	1.7	15.8	3.3	1.83	0.55
25	2.5 nm Cr	0.8	12.4	2.3	1.74	0.75
25	2.5 nm Cr	0.7	11.5	1.8	1.62	0.90

superconducting heterostructures such as Nb/Gd,<sup>17,18</sup> Nb/Fe,<sup>19,20</sup> Pb/Fe,<sup>21</sup> Nb/Cu<sub>0.43</sub>Ni<sub>0.57</sub>,<sup>22</sup> and V/Fe (Refs. 23 and 24) have allowed a good understanding of the influence of the ferromagnetic layers in a superconducting layer in close proximity. However, much less attention has been devoted to the study of heterostructures consisting of AF and superconducting layers. The strong suppression of the superconducting transition temperature observed in superconductor/Cr heterostructures such as Pb/Cr,<sup>25</sup> Nb/Cr,<sup>26</sup> and V/Cr (Ref. 27) confirms that the superconductor-antiferromagnet proximity effect cannot be considered alike to the conventional proximity effect at the boundary between normal and superconducting metal layers. Then, the second part of this work is dedicated to a comparative study of the superconducting proximity effects in Nb/Cr/Fe nanoislands and Nb/normal metal/Fe-nanoislands where the normal metals used are Pt and Al. By adjusting the deposition parameters of the Fe layer, island size can be modified in a controlled fashion,<sup>28</sup> allowing the analysis of proximity effects as a function of the contact surface area between the superconductor and the ferromagnet. We show the different role that Cr plays from a normal metal, as an intermediate layer between Nb film and Fe islands.

## II. EXPERIMENTAL DETAILS

Nb/spacer/layer Fe-island samples were grown following these successive steps: first, an Fe layer was grown by means of triode sputtering ( $P_{\text{Ar}}=1 \times 10^{-4}$  mbar, 0.4 nm/min) on Al<sub>2</sub>O<sub>3</sub> (0001) substrates in a system with a base pressure in the low  $10^{-9}$  mbar range. Substrate temperature was set at 700 °C in order to favor the formation of islands since the growth of (110) oriented Fe in an islanded fashion had been previously reported<sup>29</sup> when deposited at elevated temperatures onto basal plane sapphire substrates. The (110) textured Fe islands present three in-plane equivalent azimuthal orientations ( $[1-10] \text{ Fe} \parallel \langle 11-20 \rangle \text{ Al}_2\text{O}_3$ ) due to the symmetry of the substrate.<sup>30</sup> Details about the fabrication, structure, and morphology of these islanded films can be found elsewhere.<sup>29,30</sup> Then, a 2.5 nm thick Pt, Cr, or Al spacer layer was deposited on top of the Fe nanoislands by triode sputtering, keeping the samples at room temperature to minimize intermixing. *In situ* magneto-optical transverse Kerr loops were performed on uncapped and capped Fe islands imme-

diately after deposition, keeping the samples in a base pressure in the low  $10^{-9}$  mbar. Finally, Nb layer of 25 nm nominal thickness was grown by sputtering on top of spacer/Fe nanostructures at room temperature after the *in situ* magneto-optical characterization was performed. The growth rate was 27.4 nm/min and the Ar pressure during deposition was  $8 \times 10^{-3}$  mbar.

At fixed deposition conditions, island size is controlled by the Fe deposition time<sup>28</sup> (with larger island sizes for larger nominal Fe thickness). Thus, the samples may be labeled by the nominal thickness corresponding to that of a continuous and flat Fe film if grown on the same substrate but at room temperature. Two different kinds of samples series were fabricated (see Table I). In the first one, Fe nominal thickness (and consequently island size) was fixed, while the spacer material was varied. In the second one, spacer material was fixed and islands' size changed. Additionally, two other similar series of samples were prepared. They presented similar trends in their morphological, magnetic, and superconducting properties as the samples listed in Table I, confirming the reproducibility of our results.

Finally, it is worth mentioning that two control samples were fabricated for each Nb/spacer/Fe-island trilayer grown. The first one consisted of a 25 nm Nb layer on Si (100) substrate. The aim of this control sample is to check that Nb grows in identical conditions onto all the bilayers. In fact, the superconducting transition temperature  $T_C$  was 7.4 K in all the control samples. The second control sample is a spacer/Fe-island twin bilayer grown under identical conditions as each Nb/spacer/Fe-island sample in order to perform the *ex situ* morphological characterization by atomic force microscopy (AFM).

A magneto-optical transverse Kerr effect (MOTKE) system, equipped with a closed-loop He cryostat and a 2.5 kOe electromagnet,<sup>31</sup> has been used to study the magnetic properties of the samples in the temperature range of 15–330 K. In this system the magnetic behavior of the sample is obtained from the change in reflectivity of *p*-polarized light with the magnetic field always applied in the sample plane and perpendicular to the optical plane.<sup>32</sup> Hysteresis loops were recorded first after a zero-field-cooling process and, then, after a field-cooling (FC) process from room temperature to 15 K in a field of 2.4 kOe, which is enough to saturate

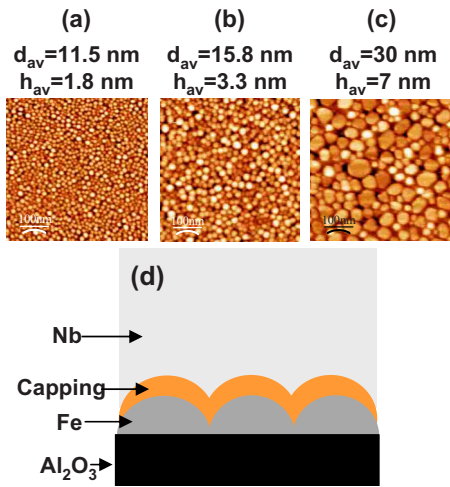


FIG. 1. (Color online) [(a)–(c)] AFM images of assemblies of Fe nanoislands deposited on sapphire substrates with different island sizes (i.e., different nominal Fe thicknesses). Labels indicate average island diameters ( $d_{av}$ ) and heights ( $h_{av}$ ). (d) Sketch of the samples structure derived from the observations.

the samples in the studied temperature range. Exchange bias field was obtained from the displacement of each hysteresis loop in comparison with the room temperature measurement.

Resistivity versus temperature curves were measured with a standard four point method in a He cryostat with a 90 kOe superconducting magnet. The superconducting transition temperature  $T_C$  was obtained from the midpoint of the transition curves,  $\rho(T_C)=0.5\rho_N$ , where  $\rho_N$  is the normal state resistivity measured at 10 K.

### III. RESULTS AND DISCUSSION

#### A. Morphological and magnetic properties of the capped Fe islands

Figure 1 shows typical AFM images of several high temperature grown Fe samples, evidencing in all the cases a morphology composed of islands with rounded tops [average in-plane diameter ( $d$ ) and average height ( $h$ ) are shown next to each topography image]. Average island size varies from  $d=10$  nm and  $h=1$  nm up to  $d=60$  nm and  $h=7$  nm, depending on the deposition time. The samples with smaller islands [Fig. 1(a)] show a homogeneous size distribution. By increasing the amount of deposited iron, the islands become larger, filling the substrate completely. Lateral island growth is limited by the presence of neighboring islands that coalesce for higher deposition times, giving rise to a wider distribution of islands size. As can be seen in Fig. 1(c) small rounded islands coexist with larger islands that are formed by the coalescence of smaller ones. It is interesting to mention that AFM measurements performed in both capped and uncapped samples yield very similar morphologies and island sizes which evidence the conformal nature of the capping materials. A sketch of the resulting Nb/capping/Fe-island sample morphology is shown in Fig. 1(d).

The data extracted from the AFM characterization of the samples are listed in the fourth and fifth columns of Table I. Due to its three dimensional structure, the total surface of an Fe-island sample ( $S_{isl}$ ) can be significantly larger than the

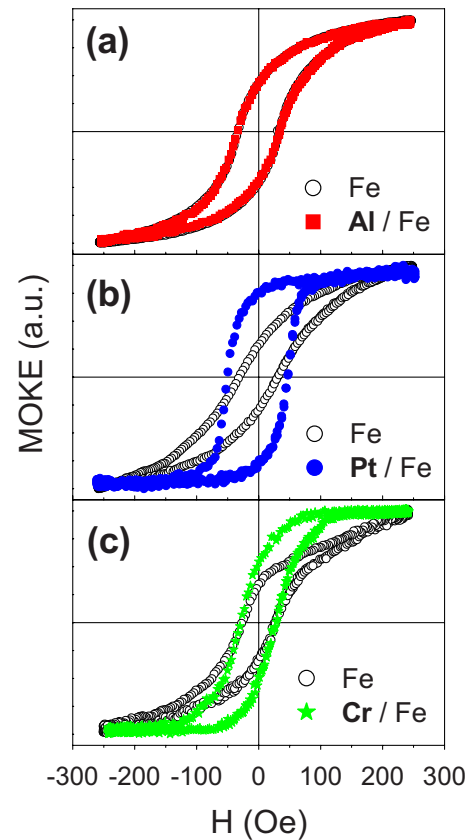


FIG. 2. (Color online) Normalized *in situ* transverse Kerr loops for uncapped Fe islands (open symbols) with 12.5 nm average diameter and covered with (a) 2.5 nm Al, (b) 2.5 nm Pt, and (c) 2.5 nm Cr spacer layers (solid symbols).

surface of the flat substrate ( $S_{subs}$ ). The ratio  $S_{isl}/S_{subs}$  can be estimated using, as a first approximation, a cylindrical island model  $S_{isl}/S_{subs}=1+4h/d$  (see sixth column of Table I). It is found that this parameter  $S_{isl}/S_{subs}$ , which can play a fundamental role in modulating the proximity effect with the Nb layer, clearly increases with island diameter. Another important parameter in nanostructured samples is the surface to volume ratio ( $S_{isl}/V_{isl}$ ) that can be estimated using again a cylindrical island approximation  $S_{isl}/V_{isl}=1/h+4/d$  (last column of Table I). In this case, it is found that  $S_{isl}/V_{isl}$  is enhanced for the smaller island sizes.

Normalized *in situ* MOTKE loops for Fe islands before and after the deposition of three different spacers are shown in Fig. 2. The three samples have the same average island diameter (12.5 nm) and their spacer layers show different magnetic behaviors: magnetic polarizable (Pt), paramagnetic and nonpolarizable (Al), and AF in the bulk state (Cr). The Kerr loops measured before the spacer layer is deposited (hollow symbols) present a ferromagnetic character (indicative of island contact) but with rounded shape and relatively low remanence, which can be understood in terms of the size distribution (and, therefore, switching field distribution) of the assembly of weakly coupled Fe nanoislands. The deposition of the Al layer onto the Fe islands [Fig. 2(a)] does not modify their magnetic behavior, whereas the deposition of the 2.5 nm Pt layer [Fig. 2(b)] leads to the appearance of a more square loop with a sharp reversal of the magnetization

and higher remanence. For the Cr capped islands [Fig. 2(c)] an intermediate behavior is obtained with remanence and coercivity larger than for the uncapped Fe islands but lower than for the Pt capped island case.

The enhanced remanence and coercivity of the Pt capped Fe islands indicate a larger collective switching of the magnetization of the islands, which can be understood as a consequence of the magnetic connection between the Fe islands mediated by the Pt spacer layer.<sup>14</sup> This can be attributed to the magnetic polarization of Pt at the interface with the Fe islands. In particular, it has been found<sup>28</sup> that the thickness of the polarized Pt layer was  $\sim 1$  nm, also in agreement with studies performed on Pt/Fe multilayers and Pt films deposited on Fe.<sup>33,34</sup> Unlike the Pt, Al is not magnetically polarizable and therefore this material does not increase the exchange interactions between islands as can be observed by comparing Figs. 2(a) and 2(b).

The different behaviors shown in Figs. 2(a) and 2(c) between Al and Cr spacer layers onto Fe nanoislands can be understood in the hypothesis that magnetic order is present in the 2.5 nm Cr thick layer. On the other hand from the comparison of Figs. 2(b) and 2(c) it can be seen that the Cr layer induces an observable interisland coupling but not as strong as in the Pt case. It is important to emphasize that, although the hysteresis loops of Pt/Fe and Cr/Fe are very similar, the mechanisms by which the Pt and Cr increase the interactions between islands are different for both materials: Pt is a paramagnetic material in which the coupling is related to the polarization of the interface region by the Fe islands and, in the case of the Cr, this element is an antiferromagnet in the bulk state that can couple the Fe islands via exchange interactions. Thus, the lower remanence values of the Cr/Fe-island system could be related to frustration effects caused by the oscillatory nature of Fe–Cr–Fe coupling<sup>1</sup> in the complex Cr/Fe-island geometry (similar to the effect of roughness in Fe/Cr multilayers<sup>35,36</sup>).

A good probe of AF order in the Cr layers of Fe/Cr samples can be taken from exchange bias measurements,<sup>37,38</sup> that is, from the presence of a field shift of the hysteresis loop in materials composed of ferromagnetic-AF interfaces after a FC process from above the Néel temperature of the antiferromagnet.<sup>39–41</sup> Figure 3(a) shows two hysteresis loops measured at 320 and 165 K after cooling with an applied field of 2.4 kOe for a sample with a 2.5 nm thick Cr layer and Fe-island size  $d=12.5$  nm. The lower temperature loop has a larger coercivity and is clearly shifted to negative fields in comparison to the 320 K loop, revealing the presence of AF order in the 2.5 nm Cr layer. It is important to note the role played by the roughness in the samples studied in this work, which promotes exchange bias at smaller nominal Cr thickness than has been reported in the literature.<sup>2</sup>

Figure 3(b) shows the temperature dependence of the exchange bias field ( $H_E$ ) for a series of samples with 2.5 nm thick Cr layers and Fe islands with diameter ranging from 11.5 to 30 nm. Also included for comparison are the results obtained in a 2.5 nm Cr/0.8 nm Fe film, in which the Fe layer has been grown at room temperature to obtain a continuous film and has the same nominal thickness as the sample with 12.5 nm island size. For all the samples, it is found that  $H_E$  is

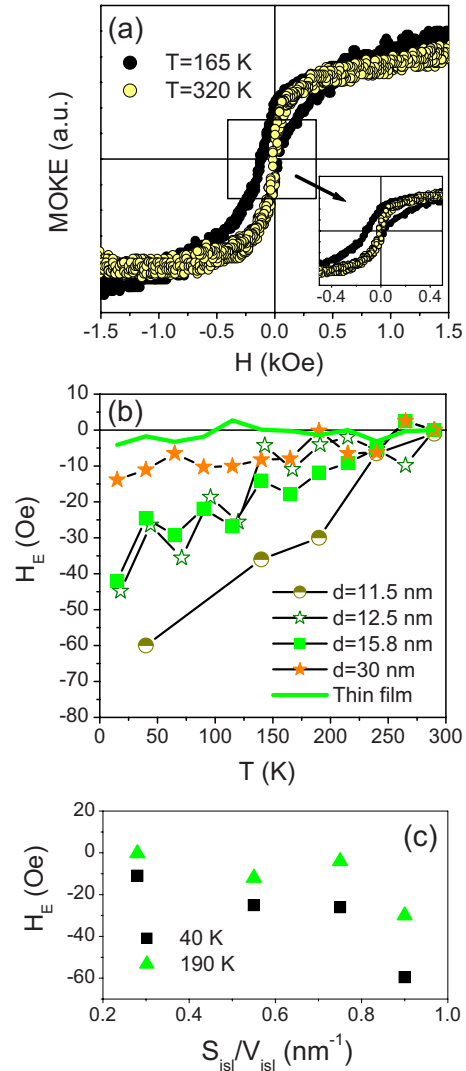


FIG. 3. (Color online) (a) Hysteresis loops of a sample with a 2.5 nm thick Cr layer and Fe-island size  $d=12.5$  nm measured at 320 and 165 K after a FC process. (b) Temperature dependences of the exchange bias in 2.5 nm Cr/0.8 nm Fe film (thick solid line) and in a series of samples with a 2.5 nm thick Cr layer and Fe-island diameter in the range  $d=11.5$ –30 nm (thin solid lines are guides for the eyes). (c) Exchange bias field as a function of  $S_{\text{isl}}/V_{\text{isl}}$  for some selected temperatures.

maximum at low temperatures and decreases smoothly as the temperature increases toward room temperature. Also, in the Fe-island samples  $H_E$  is enhanced as island size becomes smaller. One possibility of understanding this size dependence of exchange bias can be the increase in the surface to volume ratio in the islands as diameter is reduced. In the limit of infinite anisotropy, the bias field of an Fe/Cr bilayer would be given by

$$H_E = J_{\text{ex}} S_{\text{Fe}} S_{\text{Cr}} / M_S t_{\text{Fe}}, \quad (1)$$

where  $J_{\text{ex}}$  is the exchange energy per unit area,  $S_{\text{Fe}}$  and  $S_{\text{Cr}}$  are the individual Fe and Cr spins,  $M_S$  is the saturation magnetization of the Fe layer, and  $t_{\text{Fe}}$  is the ferromagnetic layer thickness.<sup>42</sup> In a nanostructured sample, such as the Cr/Fe-islands, Eq. (1) is modified as<sup>43</sup>

$$H_E = (J_{\text{ex}} S_{\text{Fe}} S_{\text{Cr}} / M_S) (S_{\text{isl}} / V_{\text{isl}}), \quad (2)$$

reflecting the energy balance of the term associated to Fe–Cr exchange interactions (proportional to  $S_{\text{isl}}$ ) in comparison to the Zeeman term (proportional to  $V_{\text{isl}}$ ). This Eq. (2) is equivalent to the size dependence of exchange bias inversely proportional to nanoparticle diameter reported in spherical core-shell nanoparticles.<sup>44</sup> A plot of  $H_E$  versus  $S_{\text{isl}}/V_{\text{isl}}$  [see Fig. 3(c)] shows an increasing trend of the bias field as a function of this parameter although it is hard to confirm a simple linear relationship between both quantities as suggested by Eq. (2) from the available data.

It is interesting to note that in the results shown in Fig. 3, no measurable exchange bias is observed for the continuous 0.8 nm Fe film. Actually, measurements in continuous Cr/0.8 nm Fe bilayers as a function of Cr thickness only resulted in a significant exchange bias ( $H_E=4$  Oe at 20 K) for Cr layers thicker than 7 nm. This is consistent with previous reports in continuous Permalloy/Cr bilayers<sup>37</sup> that found a critical thickness for the observation of exchange bias above a 6 nm (much larger than our 2.5 nm Cr spacer layer thickness). The exchange bias field value ( $H_E$ ) vanishes for very thin AF films. This behavior has been associated to a reduced anisotropy in the antiferromagnet<sup>45</sup> and to a loss of AF order for very thin Cr layers [such as found in V/Cr and V/Cr/Fe multilayers for Cr thicknesses below 4 nm (Refs. 6, 7, and 46)]. However, the nanoparticle geometry seems to promote exchange bias, as reported in experiments with oxidized Co nanoparticles.<sup>47,48</sup> In the present case, the smaller critical thickness for the observation of exchange bias obtained in the Cr capped Fe-nanoisland samples in comparison with the continuous Fe/Cr bilayers can be attributed to an increase in the effective Cr thickness in the interparticle regions, in a similar way as reported in experiments of core-shell nanoparticles as a function of coverage.<sup>47</sup> This can increase the effective volume of blocked antiferromagnet above the threshold needed for the observation of exchange bias,<sup>49</sup> explaining the smaller critical thickness of the Cr layer in the nanoisland geometry. Also, the smaller volume of the ferromagnetic nanoislands, and its corresponding reduction in Zeeman energy in comparison with the anisotropy energy of the antiferromagnet, should enhance the observed exchange bias field.

## B. Proximity effect in the Nb/spacer/Fe-island samples

Proximity effect between superconductors and normal metals or magnetic materials provides another way to explore the presence of AF order in the 2.5 nm Cr layer deposited on the top of Fe nanoisland. Figure 4 shows the resistivity superconducting transitions for several Nb/spacer/Fe-island sample series in which island size is varied for the different kinds of spacers studied: 2.5 nm Al for the samples in Fig. 4(a), 2.5 nm Pt in Fig. 4(b), and 2.5 nm Cr in Fig. 4(c). In the first two cases, i.e., for Al and Pt spacer layers, a similar trend is observed with a strong decrease in superconducting transition temperature as island size increases from  $d=12.5$  nm to  $d=30$  nm. On the contrary, for the Cr capped Fe islands an increasing trend of  $T_C$  with island size is ob-

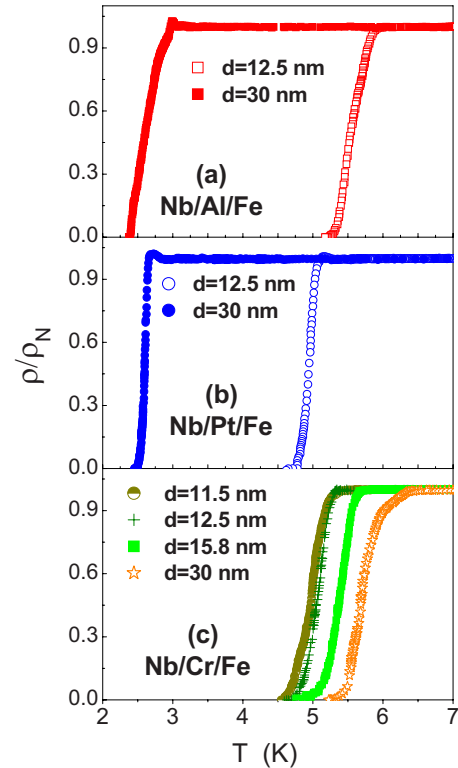


FIG. 4. (Color online) Temperature dependence of the resistivities of several Nb/spacer/Fe-island samples with identical spacer material and different island sizes: (a) 25 nm Nb/2.5 nm Al/Fe island with  $d=12.5$  nm (hollow symbols) and  $d=30$  nm (filled symbols); (b) 25 nm Nb/2.5 nm Pt/Fe island with  $d=12.5$  nm (hollow symbols) and  $d=30$  nm (filled symbols); and (c) 25 nm Nb/2.5 nm Cr/Fe island with  $d=11.5$  nm (filled circles), 12.5 nm (hollow stars), 15.8 nm (hollow squares), and 30 nm (filled stars). All the curves have been normalized by their normal state resistivity  $\rho_N$  measured at 10 K.

served, from  $T_C=5.0$  K for the smallest 11.5 nm islands to  $T_C=5.7$  K for the largest 30 nm islands. That is, the effects of the paramagnetic Al and Pt interlayers in the proximity effect between the Fe islands and the top Nb layer are very similar, whereas an opposite behavior appears when a Cr spacer layer is introduced in between the superconductor and the Fe islands due to the presence of AF order.

Considering first the samples with Al or Pt spacer layers, it must be taken into account that both of them are normal metals. Thus, the distance over which Cooper pairs diffuse into the normal metal, i.e., the normal-metal coherence length  $\xi_N$ , is typically on the order of several tens of nanometers<sup>50</sup> near  $T_C$ . This is important since, for example, in proximity effect experiments performed in continuous Nb/Pt/Fe trilayers<sup>51</sup> it was found that  $\xi_N$  is the characteristic length scale for the screening of the pair breaking effects induced by Fe layer across a Pt interlayer (which was about 30 nm in that case). Therefore, the much thinner 2.5 nm Al or Pt layers that cover the Fe islands in our experiment must be quite transparent to the penetration of Cooper pairs across them. In this sense, the relevant proximity effect takes place mainly between the Nb layer and the Fe islands. For this reason, the overall behaviors obtained for both spacer materials are very similar: a decrease in  $T_C$  as island size becomes larger. There are two main parameters that increase with island size and that may be responsible for the observed en-

hancement of the proximity effect: one of them is Fe thickness and the other is the exposed Fe islands' surface (characterized by the ratio  $S_{\text{isl}}/S_{\text{subs}}$  in Table I). In proximity effect measurements in Nb/Fe multilayer systems<sup>19,20,52</sup> one of the key parameters that determines the multilayer  $T_C$  is Fe layer thickness  $t_{\text{Fe}}$ :  $T_C$  versus  $t_{\text{Fe}}$  curves show a very pronounced decrease up to  $t_{\text{Fe}}$  of about 1.5 nm, with a possible nonmonotonic behavior in the 0.7–1.5 nm range,<sup>19</sup> but then level off to a constant low  $T_C$  value for  $t_{\text{Fe}}$  above 1.5 nm. This relatively short length scale for the proximity effect in Nb/Fe multilayers is set by the small size of the coherence length in the ferromagnet,  $\xi_{\text{Fe}}$  (typically on the order 0.1–1 nm)<sup>23,53</sup> and by the possible presence of Fe dead layers of thickness below 1 nm.<sup>20,52</sup> In the case of Fe-island samples, the best parameter to define an effective Fe thickness can be the average island height  $h$  obtained from the AFM characterization. Particularly, for the samples in Figs. 4(a) and 4(b),  $h$  increases from  $h=2.2$  nm for small Fe islands ( $d=12.5$  nm) to  $h=7.1$  nm for large Fe islands ( $d=30$  nm). Thus, in both cases,  $h$  is significantly larger than  $\xi_{\text{Fe}}$ , so that the ferromagnetic proximity effect should be basically saturated in both samples and no essential differences in  $T_C$  should be expected for this reason.

Thus, the contact surface between the Nb film and the Fe islands appears as the relevant sample parameter for understanding the observed behavior in Fig. 4. This contact surface would be given simply by  $S_{\text{subs}}$  in an Fe/Nb bilayer but can be significantly enhanced by island morphology as indicated in Table I. Previous works on the role of interface characteristics in ferromagnetic-superconducting proximity effect have focused on the influence of interface transparency,<sup>21,23,54</sup> whereas interface roughness effects have been mainly discussed as a source of  $t_{\text{Fe}}$  distribution that averages out the fine details of the nonmonotonic proximity effect and reduces interface transparency.<sup>21</sup> In the present case, average Fe-island diameter is over 10 nm, much larger than the typical lateral length scale of roughness in thin films and the Nb mean free path and, more importantly, larger than the superconducting coherence length  $\xi_s=5.6$  nm obtained from the critical field characterization. Thus, the increase in contact area  $S_{\text{isl}}$  between the Fe islands and the Nb film implies a larger volume of the superconducting film within the proximity range of the ferromagnet, i.e., with a reduced order parameter, which results in the lower transition temperatures for the samples with larger Fe-island size observed in Figs. 4(a) and 4(b).

In this framework, the behavior of the Nb/Cr/Fe-island samples presented in Fig. 4(c) is somewhat surprising since  $S_{\text{isl}}/S_{\text{subs}}$  is enhanced in a similar way for large island sizes independently on the spacer material. However, the role that Cr plays as an intermediate layer between the Nb film and the Fe islands is quite different from a normal metal: strong reduction in the transition temperatures has been found in several superconducting/Cr multilayer systems<sup>25–27</sup> with a relatively short penetration depth of the Cooper pairs into the Cr layer (only 4 nm).<sup>6</sup> Thus, within the theory of superconducting/normal metal/ferromagnet trilayers,<sup>55</sup> the Nb/Cr/Fe samples appear at an opposite limit from Nb/Al/Fe and Nb/Pt/Fe systems: the 2.5 nm Cr spacer layer has a

strong screening effect on the Cooper pairs from the Fe islands, so that the proximity effect with the Nb layer mainly takes place due to strong pair breaking effects in the Cr layer itself and in the upper Fe layers (i.e., in the disordered spin layer at the Cr/Fe-island interface that is also responsible for the observed exchange bias in Fig. 3) instead of in the “bulk” Fe islands. Therefore, the observed decrease in transition temperature in the Nb/Cr/Fe-island samples as island size is reduced must be reflecting structural changes in the Cr/Fe interface as a function of island size. Actually, pair breaking in superconductor/Cr heterostructures has usually been attributed to strong inelastic pair breaking scattering in the Cr layer by magnetic defects.<sup>6</sup> Taking into account the corrugation and strains of the Cr spacer layer induced by the Fe islands morphology, the number of magnetic defects in the interface increases as the Fe islands become smaller, resulting in an enhanced proximity effect and lower  $T_C$  for small island sizes.

#### IV. CONCLUSIONS

In summary, the magnetic and superconducting properties of Nb/spacer/Fe-nanoisland samples have been studied as a function of spacer layer material (Al, Pt, or Cr) and island size. The magnetic correlations between Fe islands that are not affected by the deposition of an Al layer are, however, enhanced by the Pt and Cr layers. In this latter case, a significant exchange bias is observed in the Cr/Fe-island structures, which increases as island size is reduced, and with a Cr spacer layer only 2.5 nm thick, (i.e., much lower than the critical thickness reported in multilayer films), indicating the presence of AF order for these thin Cr layers.

The superconducting transition temperatures of the Nb layers grown on top of the Fe islands present different trends as a function of island size depending on the magnetic or nonmagnetic character of the spacer material, more specifically, depending on the relation between the Cooper pairs penetration depth and spacer layer thickness. In the case of Al and Pt, the 2.5 nm spacer layer is basically transparent to the Cooper pairs, and the proximity effect is enhanced for larger island sizes. This could be related to the increase in contact area between the superconducting film and the ferromagnetic Fe islands. An opposite behavior is found for the Nb/Cr/Fe-island structures, which can be associated with the much shorter penetration depth of the Cooper pairs into the AF Cr layer, so that pair breaking takes place at magnetic defects located in the Cr layer itself and in the disordered Cr/Fe interface.

#### ACKNOWLEDGMENTS

Work was supported by Spanish Ministerio de Educación y Ciencia under Grant Nos. NAN2004-09087, FIS2005-07392, FIS2008-06249, Consolider CSD2007-00010, Consolider-Ingenio-2007 Nanoselect 26400, and MAT2005-05524-C02 and Comunidad de Madrid under Grant Nos. 2006-CM-ESP-0337-0505 (CITECNOMIK) and S-0505/MAT/0194 NANOMAGNET. O.F.d.L. wants to thank Banco Santander–UCM for a sabbatical professorship and the Brazilian science agencies FAPESP and CNPq for the partial

support. Y.H. acknowledges the program “Ramón y Cajal.”

- <sup>1</sup>P. Grünberg, R. Schreiber, Y. Pang, M. B. Brodsky, and H. Sowers, *Phys. Rev. Lett.* **57**, 2442 (1986); M. N. Baibich, J. M. Broto, A. Fert, F. Nguyen Van Dau, F. Petroff, P. Etienne, G. Creuzet, A. Friederich, and J. Chazelas, *ibid.* **61**, 2472 (1988).
- <sup>2</sup>E. E. Fullerton, K. T. Riggs, C. H. Sowers, S. D. Bader, and A. Berger, *Phys. Rev. Lett.* **75**, 330 (1995).
- <sup>3</sup>J. Meererschaut, J. Dekoster, R. Schad, P. Belien, and M. Rots, *Phys. Rev. Lett.* **75**, 1638 (1995).
- <sup>4</sup>A. Schreyer, C. F. Majkrzak, T. Zeidler, T. Schmitte, P. Bödeker, K. Theis-Bröhl, A. Abromeit, J. A. Dura, and T. Watanabe, *Phys. Rev. Lett.* **79**, 4914 (1997).
- <sup>5</sup>E. Fawcett, *Rev. Mod. Phys.* **60**, 209 (1988).
- <sup>6</sup>I. A. Garifullin, D. A. Tikhonov, N. N. Garif'yanov, and M. Z. Fattakhov, *Phys. Rev. B* **70**, 054505 (2004).
- <sup>7</sup>K. Mibu, E. Almokhtar, A. Nakanishi, T. Kobayashi, and T. Shinjo, *J. Magn. Magn. Mater.* **226–230**, 1785 (2001).
- <sup>8</sup>R. S. Fishman, *J. Phys.: Condens. Matter* **13**, R235 (2001).
- <sup>9</sup>A. B. Klautau and S. B. Legoas, *Phys. Rev. B* **60**, 3421 (1999).
- <sup>10</sup>E. J. Escorcia-Aparicio, J. H. Wolfe, H. J. Choi, W. L. Ling, R. K. Kawakami, and Z. Q. Qui, *Phys. Rev. B* **59**, 11892 (1999).
- <sup>11</sup>H. Fritzsche, S. Bonn, J. Hauschild, J. Klenke, K. Prokes, and G. J. McIntyre, *Phys. Rev. B* **65**, 144408 (2002).
- <sup>12</sup>D. Venus and B. Heinrich, *Phys. Rev. B* **53**, R1733 (1996).
- <sup>13</sup>D. Stoeffler, K. Ounadjela, J. Sticht, and F. Gautier, *Phys. Rev. B* **49**, 299 (1994).
- <sup>14</sup>E. Navarro, Y. Huttel, C. Clavero, G. Armelles, and A. Cebollada, *Appl. Phys. Lett.* **84**, 2139 (2004).
- <sup>15</sup>Y. Huttel, E. Navarro, N. D. Telling, G. Van der Laan, F. Pigazo, F. J. Palomares, C. Quintana, E. Roman, G. Armelles, and A. Cebollada, *Phys. Rev. B* **78**, 104403 (2008).
- <sup>16</sup>A. I. Buzdin, *Rev. Mod. Phys.* **77**, 935 (2005).
- <sup>17</sup>C. Strunk, C. Sürgers, U. Paschen, and H. v. Löhneysen, *Phys. Rev. B* **49**, 4053 (1994).
- <sup>18</sup>J. S. Jiang, D. Davidovic, D. H. Reich, and C. L. Chien, *Phys. Rev. Lett.* **74**, 314 (1995).
- <sup>19</sup>T. Mühge, N. N. Garif'yanov, Y. V. Goryunov, G. G. Khaliullin, L. R. Tagirov, K. Westerholt, I. A. Garifullin, and H. Zabel, *Phys. Rev. Lett.* **77**, 1857 (1996).
- <sup>20</sup>G. Verbanck, C. D. Potter, V. Metlushko, R. Schad, V. V. Moshchalkov, and Y. Bruyseraede, *Phys. Rev. B* **57**, 6029 (1998).
- <sup>21</sup>L. Lazar, K. Westerholt, H. Zabel, L. R. Tagirov, Y. V. Goryunov, N. N. Garif'yanov, and I. A. Garifullin, *Phys. Rev. B* **61**, 3711 (2000).
- <sup>22</sup>Y. V. Fominov, N. M. Chitchev, and A. A. Golubov, *Phys. Rev. B* **66**, 014507 (2002).
- <sup>23</sup>J. Aarts, J. M. E. Geers, E. Brük, A. A. Golubov, and R. Coehoorn, *Phys. Rev. B* **56**, 2779 (1997).
- <sup>24</sup>I. A. Garifullin, D. A. Tikhonov, N. N. Garif'yanov, L. Lazar, Y. V. Goryunov, S. Y. Khlebnikov, L. R. Tagirov, K. Westerholt, and H. Zabel, *Phys. Rev. B* **66**, 020505(R) (2002).
- <sup>25</sup>J. J. Hauser, H. C. Theueret, and N. R. Werthamer, *Phys. Rev.* **142**, 118 (1966).
- <sup>26</sup>Y. Cheng and M. B. Stearns, *J. Appl. Phys.* **67**, 5038 (1990).
- <sup>27</sup>M. Hübener, D. A. Tikhonov, I. A. Garifullin, K. Westerholt, and H. Zabel, *J. Phys.: Condens. Matter* **14**, 8687 (2002).
- <sup>28</sup>E. Navarro, Y. Huttel, C. Clavero, A. Cebollada, and G. Armelles, *Phys. Rev. B* **69**, 224419 (2004).
- <sup>29</sup>J. L. Menéndez, G. Armelles, C. Quintana, and A. Cebollada, *Surf. Sci.* **482–485**, 1135 (2001).
- <sup>30</sup>C. Quintana, J. L. Menéndez, Y. Huttel, M. Lancin, E. Navarro, and A. Cebollada, *Thin Solid Films* **434**, 228 (2003).
- <sup>31</sup>R. Morales and J. M. Alameda, *IEEE Trans. Magn.* **37**, 2305 (2001).
- <sup>32</sup>C. Dehesa-Martinez, L. Blanco-Gutierrez, M. Velez, J. Diaz, L. M. Alvarez-Prado, and J. M. Alameda, *Phys. Rev. B* **64**, 024417 (2001).
- <sup>33</sup>W. J. Antel, Jr., M. M. Schwickert, T. Lin, W. L. O'Brien, and G. R. Harp, *Phys. Rev. B* **60**, 12933 (1999).
- <sup>34</sup>R. Bertacco and F. Ciccaci, *Phys. Rev. B* **57**, 96 (1998).
- <sup>35</sup>D. T. Pierce, J. Unguris, R. J. Celotta, and M. D. Stiles, *J. Magn. Magn. Mater.* **200**, 290 (1999).
- <sup>36</sup>E. E. Fullerton, D. M. Kelly, J. Guimpel, I. K. Schuller, and Y. Bruyseraede, *Phys. Rev. Lett.* **68**, 859 (1992).
- <sup>37</sup>J. S. Parker, L. Wang, K. A. Steiner, P. A. Crowell, and C. Leighton, *Phys. Rev. Lett.* **97**, 227206 (2006).
- <sup>38</sup>F. Y. Yang and C. L. Chien, *J. Appl. Phys.* **93**, 6829 (2003).
- <sup>39</sup>J. Nogués and I. K. Schuller, *J. Magn. Magn. Mater.* **192**, 203 (1999).
- <sup>40</sup>I. K. Schuller, *MRS Bull.* **29**, 642 (2004).
- <sup>41</sup>J. F. Bobo, L. Gabillet, and M. Bibes, *J. Phys.: Condens. Matter* **16**, S471 (2004).
- <sup>42</sup>W. H. Meiklejohn and C. P. Bean, *Phys. Rev.* **105**, 904 (1957).
- <sup>43</sup>J. Nogués, J. Sort, V. Langlais, V. Skumryev, S. Suriñach, J. S. Muñoz, and M. D. Baró, *Phys. Rep.* **422**, 65 (2005).
- <sup>44</sup>O. Iglesias, A. Labarta, and X. Batlle, *J. Nanosci. Nanotechnol.* **8**, 2761 (2008).
- <sup>45</sup>Ch. Binek, H. Hochstrat, and V. Kleeman, *J. Magn. Magn. Mater.* **234**, 353 (2001).
- <sup>46</sup>M. Almokhtar, K. Mibu, A. Nakanishi, T. Kobayashi, and T. Shinjo, *J. Phys.: Condens. Matter* **12**, 9247 (2000).
- <sup>47</sup>J. Nogués, V. Skumryev, J. Sort, S. Stoyanov, and D. Givord, *Phys. Rev. Lett.* **97**, 157203 (2006).
- <sup>48</sup>A. N. Dobrynin, D. N. Ievlev, C. Hendrich, K. Temst, P. Lievens, U. Hörmann, J. Verbeeck, G. Van Tendeloo, and A. Vantomme, *Phys. Rev. B* **73**, 245416 (2006).
- <sup>49</sup>M. S. Lund, W. A. A. Macedo, K. Liu, J. Nogués, I. K. Schuller, and C. Leighton, *Phys. Rev. B* **66**, 054422 (2002).
- <sup>50</sup>H. Courtois, Ph. Gandit, and B. Pannetier, *Phys. Rev. B* **52**, 1162 (1995).
- <sup>51</sup>M. Vélez, C. Martínez, A. Cebollada, F. Briones, and J. L. Vicent, *J. Magn. Magn. Mater.* **240**, 580 (2002).
- <sup>52</sup>Th. Mühge, K. Theis-Bröhl, K. Westerholt, H. Zabel, N. N. Garif'yanov, Yu. V. Goryunov, I. A. Garifullin, and G. G. Khaliullin, *Phys. Rev. B* **57**, 5071 (1998).
- <sup>53</sup>A. Bagrets, C. Lacroix, and A. Vedyayev, *Phys. Rev. B* **68**, 054532 (2003).
- <sup>54</sup>C. Cirillo, S. L. Prischepa, M. Salvato, C. Attanasio, M. Hesselberth, and J. Aarts, *Phys. Rev. B* **72**, 144511 (2005).
- <sup>55</sup>B. P. Vodopyanov, L. R. Tagirov, H. Z. Durusoy, and A. V. Berezhnov, *Physica C* **366**, 31 (2001).